Fabrication and Photocatalytic Activity of Ag$_3$PO$_4$/T-ZnOw Heterostructures

Jianke Tang[1,2], Rongqian Meng[1], Qi Wang[2], Shengjian Zhang[1] and Qiaoling Li[1*]

Abstract

The Ag$_3$PO$_4$/tetrapod-like ZnO whisker (T-ZnOw) heterostructures were prepared via a simple precipitation method. The obtained heterostructures were characterized by X-ray diffraction, scanning electron microscopy, transmission electron microscopy, high-resolution transmission electron microscopy, X-ray photoelectron spectroscopy, and UV-Vis diffuse reflectance spectroscopy. The photodegradation activity of Ag$_3$PO$_4$/T-ZnOw was evaluated by the degradation of Rhodamine B (RhB) under visible light irradiation. When the molar ratio of Ag$_3$PO$_4$ to T-ZnOw was 10% (Ag$_3$PO$_4$/T-ZnOw-2), the highest degradation efficiency (92.9%) could be achieved among the heterostructures. The photodegradation rate constant of Ag$_3$PO$_4$/T-ZnOw-2 (0.05179 min^{-1}) was 3.59 times that of T-ZnOw (0.01444 min^{-1}). Besides, the Ag$_3$PO$_4$/T-ZnOw-2 photocatalyst still possessed a degradation efficiency of 77.8% after four successive cycles. The Ag$_3$PO$_4$/T-ZnOw-2 catalyst had much higher photocatalytic activity than pure T-ZnOw and better stability and reusability than pure Ag$_3$PO$_4$. The effect of different scavengers on degradation efficiency was investigated, and the possible photocatalytic mechanism of the Ag$_3$PO$_4$/T-ZnOw photocatalyst was also put forward.

Keywords: Ag$_3$PO$_4$/T-ZnOw, Heterostructures, Visible light, Photocatalytic

Introduction

Dye wastewater pollution from the textile industries has been a major environmental issue in recent decades due to non-biodegradability and potential carcinogenicity. Currently, the researchers have explored various techniques to handle the pollutants in wastewater. Semiconductor photocatalysis technology has been considered as an effective way for the purification of polluted water [1–6]. Zinc oxide (ZnO), an environmentally friendly photocatalytic material, has been extensively studied due to its features of low cost, high controllability, and thermal and chemical stability [7–11]. Unfortunately, the wide bandgap (3.37 eV) of ZnO restrains its large-scale practical applications in visible light [12]. Furthermore, the low separation rate of the photogenerated electron-hole pairs also limits the photocatalytic performance of ZnO. For the modification of ZnO photocatalysts, an

effective strategy is to shift the absorption band from ultraviolet to visible light range, enabling absorption of more energy from solar irradiation and enhancing the utilization of solar light [13]. It is generally known that coupling ZnO with narrow bandgap semiconductors can be an effective way to absorb more energy from the solar irradiation and enhance the photocatalytic activity. Besides, the formation of heterostructures with a properly matched energy gap can also enhance the separation of charge carriers in photocatalysts. For instance, AgBr/ZnO [14], ZnO/BiOI [15], ZnO/AgI [16], Ag$_3$VO$_4$/ZnO [17], Ag$_2$CO$_3$/ZnO [18], Ag$_2$O/ZnO [19], and BiVO$_4$/ZnO [20] have been reported.

Recently, the silver orthophosphate (Ag$_3$PO$_4$) has attracted considerable attention as a promising coupling material due to a narrow band gap (about 2.4 eV) [21], which showed high photodegradation efficiency of organic pollutions in aqueous solution under visible light [22–25]. However, the Ag$_3$PO$_4$ can be reduced to Ag^0 during the photocatalytic process due to the photocorrosion of the photogenerated electrons under visible light

* Correspondence: qiaolingl@163.com
[1]School of Chemical Engineering and Technology, North University of China, Taiyuan 030051, Shanxi, People's Republic of China
Full list of author information is available at the end of the article

Tang *et al. Nanoscale Research Letters*   (2020) 15:131

Page 2 of 10

irradiation, which may decrease the structural stability and reusability, and strongly limit the long-term application for water treatment [23, 26–28]. Besides, the use of a large amount of expensive silver-containing material in the photocatalytic system strongly increased operating costs. As previously reported, the stability of Ag_3PO_4 can be enhanced by the preparation of composites over a supporting material of matched electronic structure and the composites showed excellent photocatalytic performance at the same time [27, 29–31].

In this work, we deposited Ag_3PO_4 particles on T-ZnOw surfaces by a facile in situ deposition method at room temperature. In the Ag_3PO_4/T-ZnOw composites, T-ZnOw works as a substrate, which has unique shape and structure, low density of native defects, and large specific surface areas [32–35]. The photocatalytic activities of the Ag_3PO_4/T-ZnOw composites were investigated by decomposing RhB under the irradiation of visible light, and the stability was also determined. Furthermore, the possible photocatalytic mechanism was also discussed in detail.

Methods

Materials

T-ZnOw was obtained from Chengdu Crystrealm Co. Ltd. (Chengdu, China). Silver nitrate ($AgNO_3$, > 99.8%) was purchased from Tianjin Fengchuan Chemical Reagent Co. Ltd. (Tianjin, China). Sodium phosphate dibasic dodecahydrate ($Na_2HPO_4 \cdot 12H_2O$, 99.0%) and benzoquinone (BQ) were purchased from Aladdin Reagents Company (Shanghai, China). RhB was provided by Macklin Biochemical Company (Shanghai, China). Isopropyl alcohol (IPA) was obtained from Tianjin Kemiou Chemical Co. Ltd. (Tianjin, China). Ethylenediaminetetraacetic acid disodium salt (EDTA-2Na) was purchased from Tianjin Shentai Chemical Industry Co. Ltd. (Tianjin, China). Absolute ethanol was obtained from Sinopharm Chemical Reagent Co. Ltd. (Shanghai, China). Deionized water with resistivity of $18.2\,M\Omega\,cm$ was used in all cases from an ULUPURE water purification system (Chengdu, China).

Preparation of Photocatalysts

An in situ precipitation method was employed to prepare Ag_3PO_4/T-ZnOw composites, and the molar ratios of Ag_3PO_4 to T-ZnOw were 5%, 10%, and 15%, respectively. The products were marked as Ag_3PO_4/T-ZnOw-1, Ag_3PO_4/T-ZnOw-2, and Ag_3PO_4/T-ZnOw-3, respectively. For instance, for the Ag_3PO_4/T-ZnOw-2 sample, 0.1 g T-ZnOw and 0.0440 g $Na_2HPO_4 \cdot 12H_2O$ were dispersed into 100 mL deionized water by ultrasound and then magnetic stirred. Next, 0.0626 g $AgNO_3$ dissolved in 50 mL of deionized water was slowly added to the above suspension by syringe fixed on the injection pump

under magnetically stirring. Subsequently, the reaction system was kept under stirring for 3 h. The Ag_3PO_4/T-ZnOw precipitate was collected by centrifugation, washed thoroughly with deionized water and absolute ethanol, and subsequently dried in an oven at 60 °C. For comparison, pure Ag_3PO_4 was prepared according to the same process in the absence of T-ZnOw.
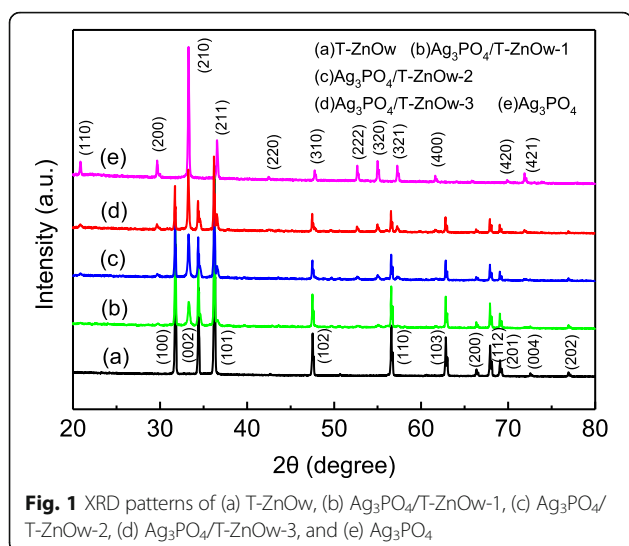
Characterization

The X-ray diffraction (XRD) measurements were carried out on a Rigaku SmartLab diffractometer using Cu K-α as the radiation with a scanning rate of 10°/min. The morphology of the composites was studied by scanning electron microscopy (SEM, JSM-7200F, JEOL, Japan). Energy-dispersive X-ray spectroscopy (EDS) attached to the SEM instrument was used to determine the chemical composition of the product. Transmission electron microscopy (TEM) and high-resolution transmission electron microscopy (HRTEM) images were obtained with a JEM-2100F transmission electron microscope. X-ray photoelectron spectroscopy (XPS) measurements were recorded on Thermo ESCALAB 250XI, and the binding energies (BEs) were calibrated with respect to the C1s peak at 284.6 eV. UV-Vis diffuse reflectance spectra (DRS) measurements were obtained by using a UV-Vis-NIR spectrophotometer (Cary5000, Agilent Technologies, USA) with polytetrafluoroethylene as the reference. Photoluminescence (PL) emission spectra of the samples were measured by F-7000 fluorescence spectrophotometer (Hitachi, Japan) with the excitation wavelength of 355 nm.

Photocatalysis Experiments

The photocatalysis experiments were tested through photodegradation of RhB under visible light. The experiments were carried out in a 250-mL jacketed glass beaker with cooling water to keep the system temperature constant at room temperature. A 300-W Xenon lamp with a 420-nm cutoff filter provided the visible light. Forty milligrams of Ag_3PO_4/T-ZnOw composite was added into 100 mL of 10 mg/L RhB solution. Before turning on the Xenon lamp, the suspensions were stirred in darkness for 30 min to reach an adsorption-desorption equilibrium. The distance between the light source and the surface of the suspensions was 15 cm. Every 10 min, 3 mL suspension was collected and centrifuged to get clear liquid then analyzed on a TU-1901 UV-Vis spectrophotometer (Puxi, China) at 554 nm. The photocatalytic degradation efficiency was calculated as the following formula:

$$\eta = (1 - C/C_0) \times 100\%$$

where C_0 is the initial concentration of RhB and C is the concentration of RhB after illumination at time t, which varies with the reaction time.
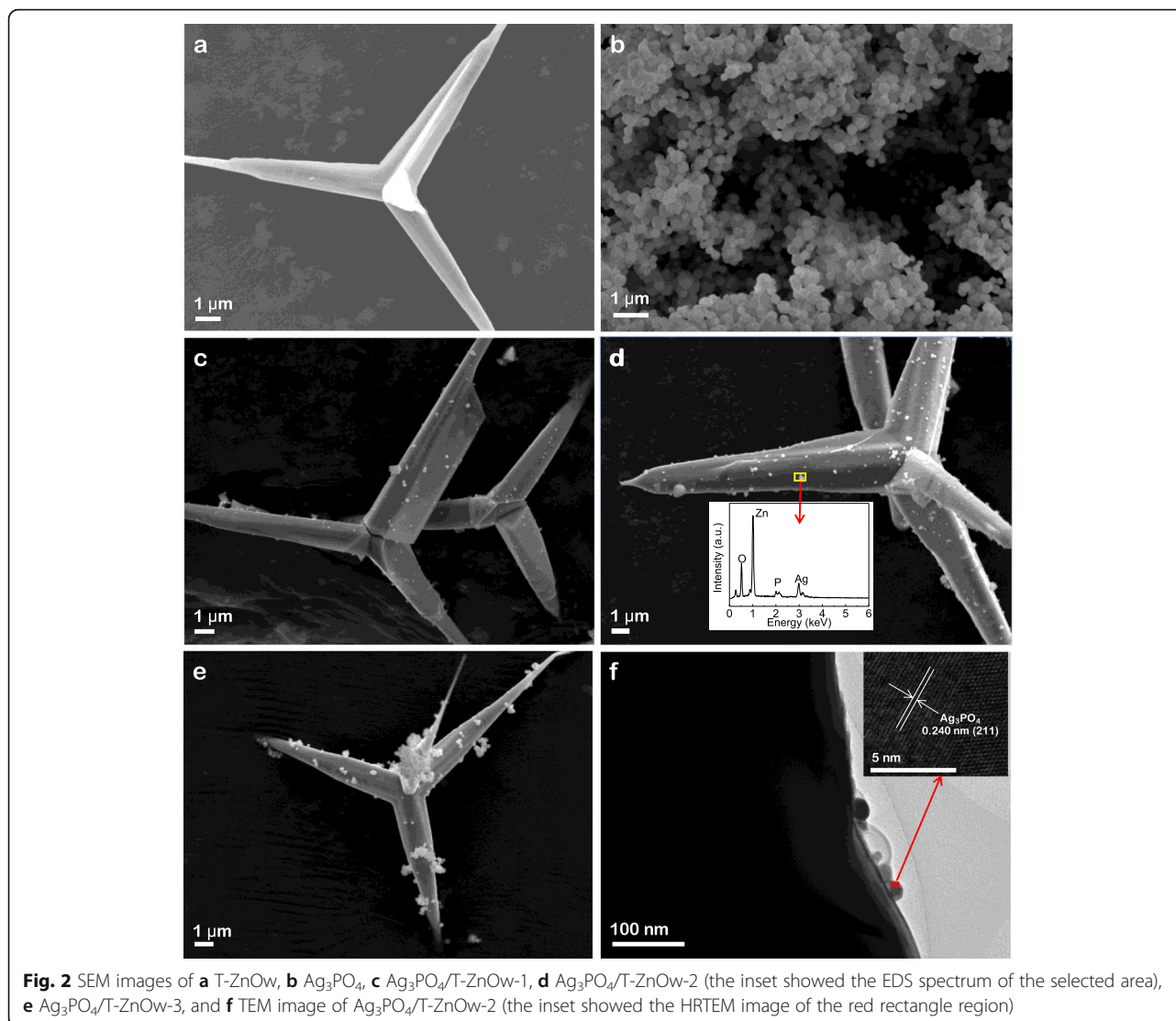
Fig. 1 XRD patterns of (a) T-ZnOw, (b) Ag$_3$PO$_4$/T-ZnOw-1, (c) Ag$_3$PO$_4$/T-ZnOw-2, (d) Ag$_3$PO$_4$/T-ZnOw-3, and (e) Ag$_3$PO$_4$

Results and Discussion

Figure 1 displayed the XRD patterns of the Ag$_3$PO$_4$/T-ZnOw composites with different molar ratios of Ag$_3$PO$_4$, together with those of T-ZnOw and Ag$_3$PO$_4$. The patterns showed that T-ZnOw was consistent with the standard pattern of ZnO of hexagonal wurtzite phase (JCPDS no. 36-1451) (Fig. 1(a)), while Ag$_3$PO$_4$ was a crystal of cubic phase (JCPDS no. 06-0505) (Fig. 1(e)). The Ag$_3$PO$_4$/T-ZnOw composites (Fig. 1(b)–(d)) exhibited a coexistence of both Ag$_3$PO$_4$ and T-ZnOw. With the molar ratios of Ag$_3$PO$_4$ increasing, the intensities of the peaks of Ag$_3$PO$_4$ enhanced markedly, whereas those of T-ZnOw decreased concurrently. The peaks of the Ag$_3$PO$_4$/T-ZnOw composites were obviously related to T-ZnOw and Ag$_3$PO$_4$, and no other new crystal phases were found, showing that loading of Ag$_3$PO$_4$ had not change the crystalline phase of T-ZnOw. These results revealed that Ag$_3$PO$_4$ particles were successfully deposited on the T-ZnOw surfaces, and Ag$_3$PO$_4$/T-ZnOw heterostructures were obtained.

Figure 2 showed the SEM images of T-ZnOw, Ag$_3$PO$_4$, and the Ag$_3$PO$_4$/T-ZnOw heterostructures, together with the TEM image and HRTEM image of Ag$_3$PO$_4$/T-ZnOw-2. T-ZnOw with fairly smooth surface had four legs growing from a common core and extending into the surrounding space. This extension facilitated assembly into a good network with mechanical strength by connecting the legs with each other. Pure Ag$_3$PO$_4$ exhibited an irregular spherical shape with a diameter of 150–500 nm. The size of T-ZnOw was at micron level, whereas the size of Ag$_3$PO$_4$ was at nanoscale level. Figure 2c–e displayed the SEM images of Ag$_3$PO$_4$/T-ZnOw heterostructures. It could be found that nano-sized Ag$_3$PO$_4$ particles were deposited on the three dimensional (3D) support framework of T-ZnOw. The amount and size of the Ag$_3$PO$_4$ particles increased with the mole

ratios of Ag$_3$PO$_4$ increasing. When the molar ratio of Ag$_3$PO$_4$ was 10%, the average diameter of Ag$_3$PO$_4$ particles was about 150 nm, while further increasing the amount of Ag$_3$PO$_4$ resulted in the aggregation of Ag$_3$PO$_4$ particles on the surface of T-ZnOw (Fig. 2e). Figure 2f was the TEM image of the contact interface of the Ag$_3$PO$_4$/T-ZnOw-2. The nano-sized Ag$_3$PO$_4$ particles were attached on the surface of T-ZnOw with a good contact. The inset showed the HRTEM image of the red rectangle region of Ag$_3$PO$_4$/T-ZnOw-2, and the lattice spacing of 0.240 nm corresponds to the (211) crystal plane of Ag$_3$PO$_4$. The inset of Fig. 2d showed the EDS spectrum corresponding to the rectangle region of the SEM image of the Ag$_3$PO$_4$/T-ZnOw-2 sample. The sample consisted of four elements, Zn, Ag, O, and P, which was in consistent with the XPS results.

XPS measurements were carried out to investigate the elemental composition and chemical states of the Ag$_3$PO$_4$/T-ZnOw-2 sample. Figure 3a exhibited the survey XPS spectrum and indicated the existence of the Zn, Ag, O, and P. Figure 3b showed the high-resolution XPS spectrum of the Zn 2p, and two binding energy peaks at 1021.5 and 1044.6 eV could be assigned to Zn 2p$_{3/2}$ and Zn 2p$_{1/2}$ of T-ZnOw, respectively [36]. Two peaks located at 367.2 and 373.2 eV could be attributed to Ag 3d$_{5/2}$ and Ag 3d$_{3/2}$ in the XPS spectrum of Ag 3d orbital (Fig. 3c), which was a characteristic of Ag$^+$ [11]. As seen from the XPS spectrum of O 1s in Fig. 3d, there were three peaks at 529.9, 531.2, and 532.5 eV, which could be ascribed to the oxygen lattices in T-ZnOw [33], Ag$_3$PO$_4$ [37], and adsorbed –OH groups on the surface of Ag$_3$PO$_4$/T-ZnOw-2, respectively. A weak and broad band centered at 132.3 eV in Fig. 3 e could be ascribed to the characteristic P 2p from Ag$_3$PO$_4$ [38]. The XPS results further proved that Ag$_3$PO$_4$ and T-ZnOw had been compounded.

UV-Vis diffuse reflectance spectra (DRS) were measured to study the optical absorption properties of the Ag$_3$PO$_4$/T-ZnOw heterostructures, together with those of T-ZnOw and Ag$_3$PO$_4$ (Fig. 4a). It could be observed that the absorption edge of T-ZnOw and Ag$_3$PO$_4$ was stated to be about 400 and 510 nm, respectively. Compared with T-ZnOw, the Ag$_3$PO$_4$/T-ZnOw heterostructures exhibited increasing absorption intensities in visible light region with the molar ratios of Ag$_3$PO$_4$ increasing. The widened absorption range and enhanced absorbance of the Ag$_3$PO$_4$/T-ZnOw heterostructures in the visible light region were benefit from the introduction of the narrower bandgap of Ag$_3$PO$_4$. The above results indicated that the Ag$_3$PO$_4$/T-ZnOw heterostructures were potential visible-light-driven photocatalysts. Furthermore, the bandgap energy of T-ZnOw and Ag$_3$PO$_4$ was evaluated by Kubelka-Munk function [39]. According to the plot of $(ahv)^2$ versus energy, as shown

Fig. 2 SEM images of **a** T-ZnOw, **b** Ag$_3$PO$_4$, **c** Ag$_3$PO$_4$/T-ZnOw-1, **d** Ag$_3$PO$_4$/T-ZnOw-2 (the inset showed the EDS spectrum of the selected area), **e** Ag$_3$PO$_4$/T-ZnOw-3, and **f** TEM image of Ag$_3$PO$_4$/T-ZnOw-2 (the inset showed the HRTEM image of the red rectangle region)

in Fig. 4b, the bandgap value of T-ZnOw and Ag$_3$PO$_4$ was about 3.16 and 2.42 eV, respectively.

Photodegradation of RhB was used to evaluate the photocatalytic activity of T-ZnOw, Ag$_3$PO$_4$/T-ZnOw-1, Ag$_3$PO$_4$/T-ZnOw-2, Ag$_3$PO$_4$/T-ZnOw-3, Ag$_3$PO$_4$, and a mixture of T-ZnOw (26.41 mg) and Ag$_3$PO$_4$ (13.59 mg) under visible light. Figure 5a showed the photocatalytic activity of different samples for RhB degradation. After irradiation for 50 min, the degradation efficiency of T-ZnOw, Ag$_3$PO$_4$/T-ZnOw-1, Ag$_3$PO$_4$/T-ZnOw-2, Ag$_3$PO$_4$/T-ZnOw-3, Ag$_3$PO$_4$, and the mixture was 52.5%, 85.3%, 92.9%, 79.9%, 96.9%, and 62.9%, respectively. The physical mixture of T-ZnOw and Ag$_3$PO$_4$ which had the same composition proportion with Ag$_3$PO$_4$/T-ZnOw-2 displayed lower degradation efficiency of RhB than that of Ag$_3$PO$_4$/T-ZnOw-2, implying that Ag$_3$PO$_4$/T-ZnOw heterostructures were formed. With the molar ratios of Ag$_3$PO$_4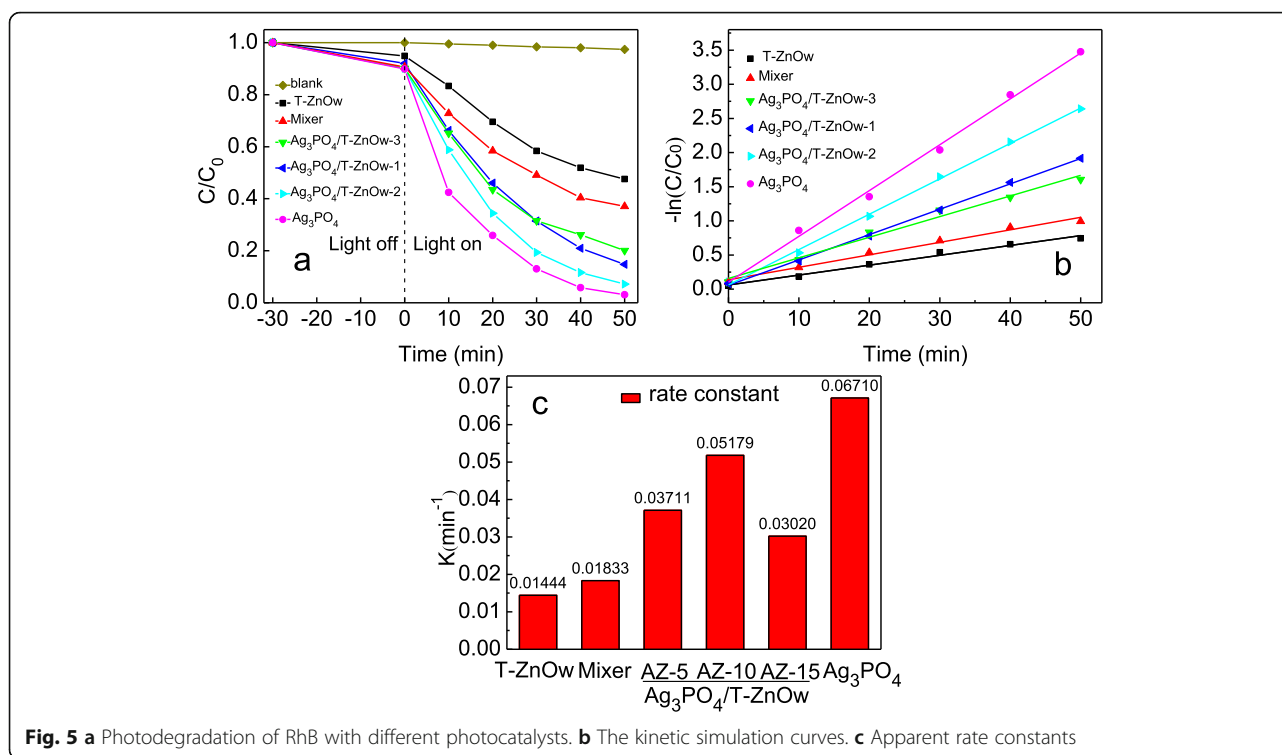$ increasing, the degradation efficiency of RhB was first increased and then decreased, and Ag$_3$PO$_4$/T-ZnOw-2 showed the highest degradation efficiency among the heterostructures, which was very closed to that of Ag$_3$PO$_4$. The agglomerated Ag$_3$PO$_4$ particles in the Ag$_3$PO$_4$/T-ZnOw-3 sample affected the size and the dispersion of Ag$_3$PO$_4$. It is well known that a smaller particle size decreases the electron-hole recombination possibility, thereby improving the photocatalytic performance of the material. In addition, the large size of Ag$_3$PO$_4$ particles in the Ag$_3$PO$_4$/T-ZnOw-3 sample may weaken the anchoring force between T-ZnOw and Ag$_3$PO$_4$ and destroy the heterojunction structure, which would limit the photocatalytic activity. The photodegradation of RhB followed the pseudo-first-order reaction, as shown in Fig. 5b. Figure 5c displayed the degradation rate constants of different photocatalysts, and the trend was the same as the degradation efficiency. The photodegradation rate constant of Ag$_3$PO$_4$/T-ZnOw-2 (0.05179 min^{-1}) was 3.59

Fig. 3 XPS spectra of Ag_3PO_4/T-ZnOw-2: **a** survey scan, **b** Zn 2p, **c** Ag 3d, **d** O1s, and **e** P 2p
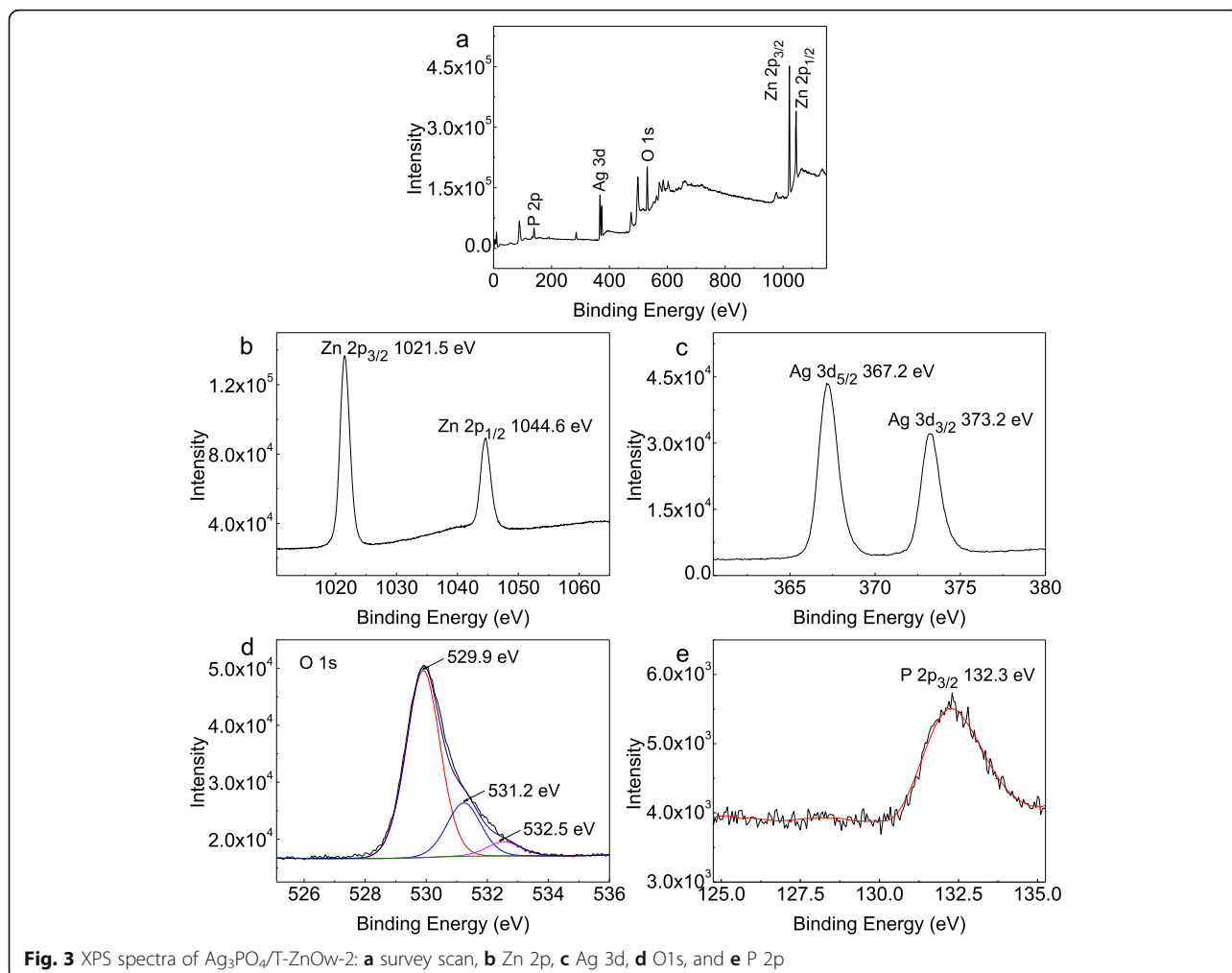
times that of T-ZnOw ($0.01444\,min^{-1}$). The above results clearly indicated that the photocatalytic activity of T-ZnOw was increased by Ag_3PO_4 modification. The improved photocatalytic activity of Ag_3PO_4/T-ZnOw heterostructures was benefited from the enhanced visible light absorbance intensity by loading Ag_3PO_4 on the surface of T-ZnOw, which would enable the Ag_3PO_4/T-ZnOw heterostructures to produce photogenerated carriers for the photodegradation of RhB under visible light. It should be noted that Ag_3PO_4 seemed to have the best photocatalytic activity among the as-prepared samples. Nevertheless, Ag_3PO_4 exhibited lower stability compared with Ag_3PO_4/T-ZnOw shown in the following discussion, which affected its long-term uses.

Fig. 4 a UV-Vis DRS of T-ZnOw, Ag_3PO_4/T-ZnOw-1, Ag_3PO_4/T-ZnOw-2, Ag_3PO_4/T-ZnOw-3, and Ag_3PO_4. **b** Plots of $(ahv)^2$ versus energy (hv)

Fig. 5 a Photodegradation of RhB with different photocatalysts. **b** The kinetic simulation curves. **c** Apparent rate constants
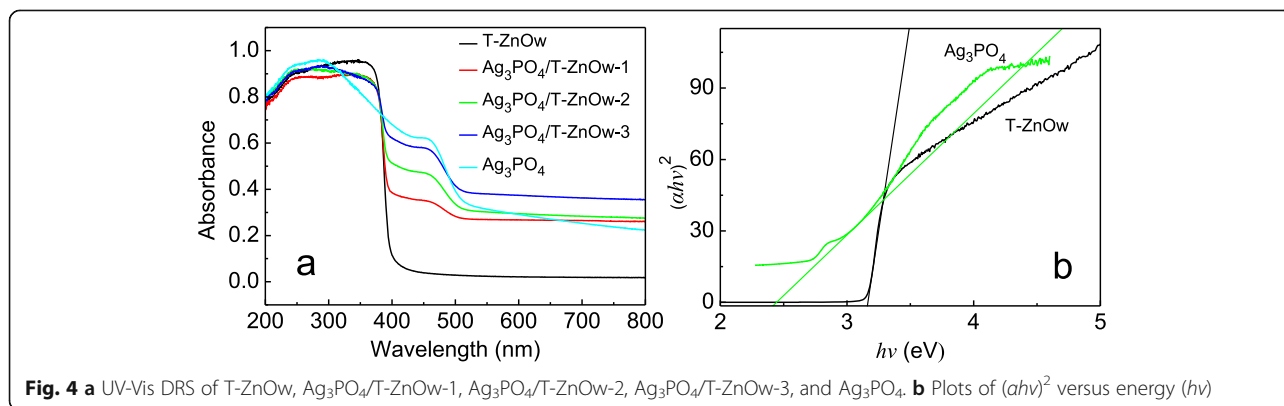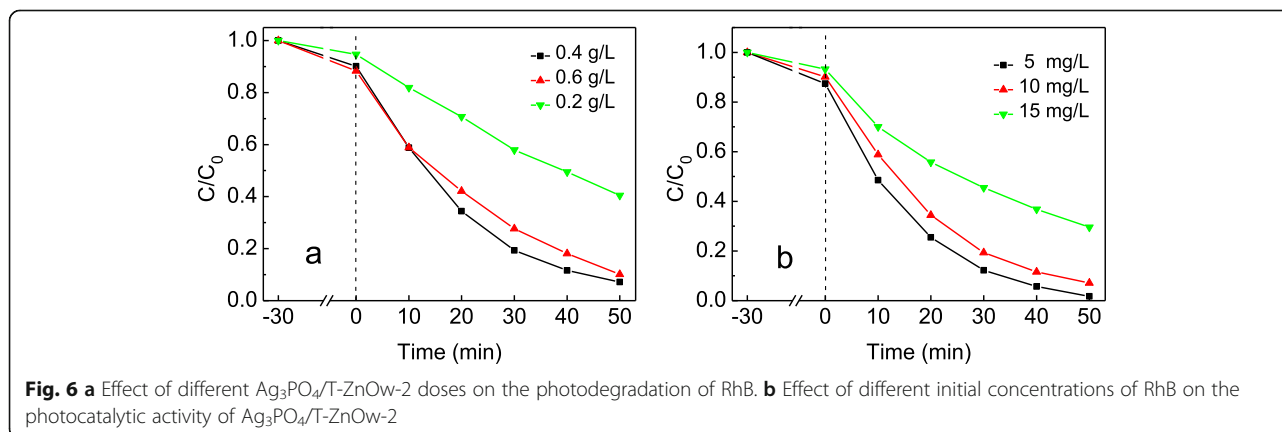
Proper doses of photocatalyst in photodegradation system can reduce cost in economic viewpoint. Figure 6a showed the influence of the feed doses of Ag_3PO_4/T-ZnOw-2 on the degradation efficiency. The degradation efficiency obviously increased with the dose increased from 0.2 to 0.4 g/L and decreased thereafter. With the increasing of catalyst doses, the solution turbidity was increased and the light penetration into the reaction system was reduced at the same time. The lower visible light absorption of photocatalyst could decrease the degradation efficiency at a greater dose of the photocatalyst [40, 41].

The effect of different initial RhB concentrations on the photocatalytic activity of Ag_3PO_4/T-ZnOw-2 was

studied and shown in Fig. 6b. When the initial concentrations were 5 mg/L, 10 mg/L, and 15 mg/L, the degradation efficiency of RhB were 98.2%, 92.9%, and 70.4%, respectively. The decrease in degradation efficiency may be due to the decrease of photons absorbed by the catalyst resulting from the increase in the path length of photons entering the solution with higher initial concentrations. Another reason may be more intermediates formed with the higher initial RhB concentrations which could form adsorption competition with initial reactants [42, 43]. However, too low initial concentration cannot fully show the photodegradation ability of the catalyst. Therefore, the initial concentration of RhB solution in the experiment was preferably 10 mg/L.

Fig. 6 a Effect of different Ag_3PO_4/T-ZnOw-2 doses on the photodegradation of RhB. **b** Effect of different initial concentrations of RhB on the photocatalytic activity of Ag_3PO_4/T-ZnOw-2

The stability and reusability of a photocatalyst are crucial to measure its practical application [44]. It is well known that the Ag_3PO_4 photocatalyst can be easily reduced to Ag by photocorrosion, which limits its long-term practical application. Figure 7 displayed the recycling experiments for degradation of RhB over Ag_3PO_4/T-ZnOw-2 and Ag_3PO_4. After four successive cycles, the degradation efficiency of Ag_3PO_4 was obviously lower than that of Ag_3PO_4/T-ZnOw-2. The results presented above demonstrated that whereas Ag_3PO_4 photocatalyst showed a somewhat higher photocatalytic activity on first use, the Ag_3PO_4/T-ZnOw heterostructures appeared to be potential for long-term applications due to the enhanced stability. Pure Ag_3PO_4 photocatalyst is unstable if there is no sacrificial reagent added in the photocatalytic process [45]. The solubility of pure Ag_3PO_4 in aqueous solution is relatively high, which results in the decrease of its stability during the photocatalytic process [25]. Ag_3PO_4 can be reduced to metallic Ag by the photogenerated electrons, and a certain amount of Ag can form the structure of Ag/Ag_3PO_4/T-ZnOw. The further photocorrosion of Ag_3PO_4 in Ag/Ag_3PO_4/T-ZnOw composite can be inhibited by the transfer of electrons from the conduction band of Ag_3PO_4 to metallic Ag [46]. After Ag_3PO_4 particles were anchored on the T-ZnOw surfaces, Ag_3PO_4 particles and T-ZnOw had intimate contact with each other, and the smooth T-ZnOw surfaces served as an ideal refuge for Ag_3PO_4 and make less amount of Ag_3PO_4 stripping in aqueous solution, which was similar to the reported Ag_3PO_4/$BiVO_4$ heterojunction [47]. Thus, Ag_3PO_4/T-ZnOw-2 heterostructure exhibited a good photocatalytic stability and possessed a degradation efficiency of 77.8% after recycling experiments.

The effect of different scavengers on degradation efficiency of RhB by Ag_3PO_4/T-ZnOw-2 is shown in Fig. 8 after irradiation for 50 min. After the addition of IPA,

Fig. 8 The influence on degradation efficiency of RhB by Ag_3PO_4/T-ZnOw-2 with different scavengers (scavenger dose = 0.2 mmol/L)
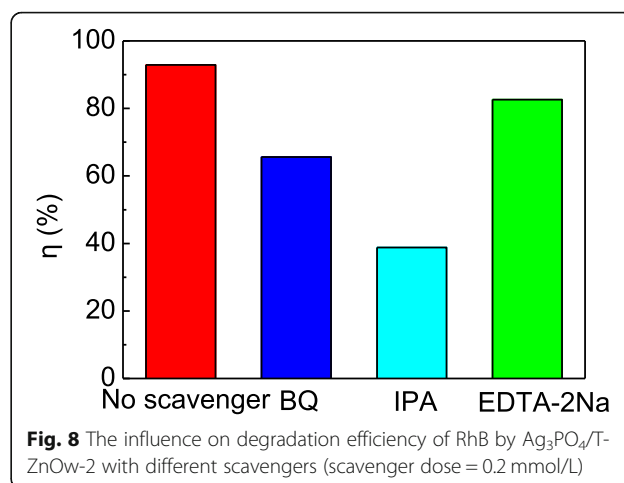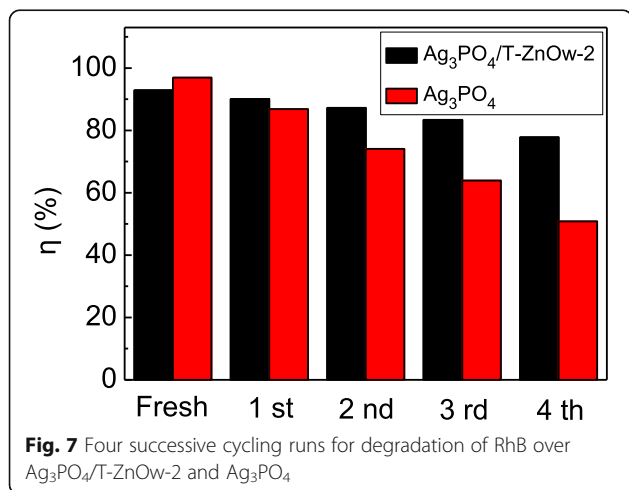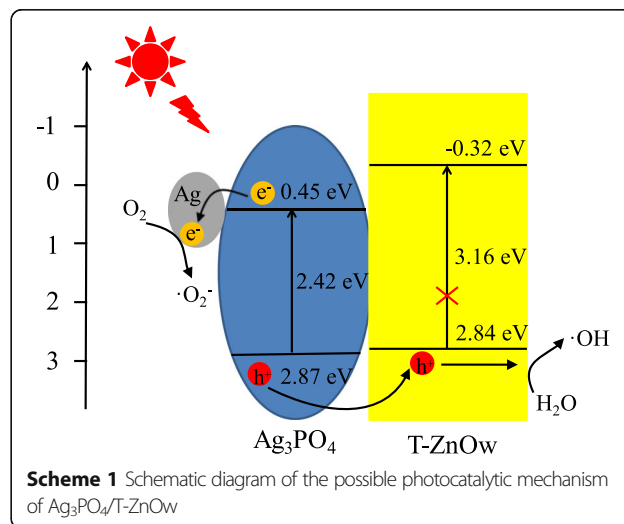
BQ, and EDTA-2Na, the degradation efficiency diminished to 38.8%, 65.6%, and 82.6%, respectively, indicating that hydroxyl radicals (·OH) and superoxide radicals (·O_2^-) were the mainly active species, and holes (h^+) played partially in the photocatalytic decoloration. The band position of Ag_3PO_4 and T-ZnOw was calculated by the following equation [18]:

$$E_{VB} = X - E^0 + 0.5E_g$$
$$E_{CB} = E_{VB} - E_g$$

where X is the absolute electronegativity of the semiconductor and E_g is the bandgap energy. The X value for Ag_3PO_4 and ZnO are 6.16 [48] and 5.76 eV [49], respectively. According to the bandgap achieved in Fig. 4, the E_{VB} of Ag_3PO_4 and T-ZnOw was calculated to be 2.87 and 2.84 eV, and their homologous E_{CB} was 0.45 and − 0.32 eV, respectively.
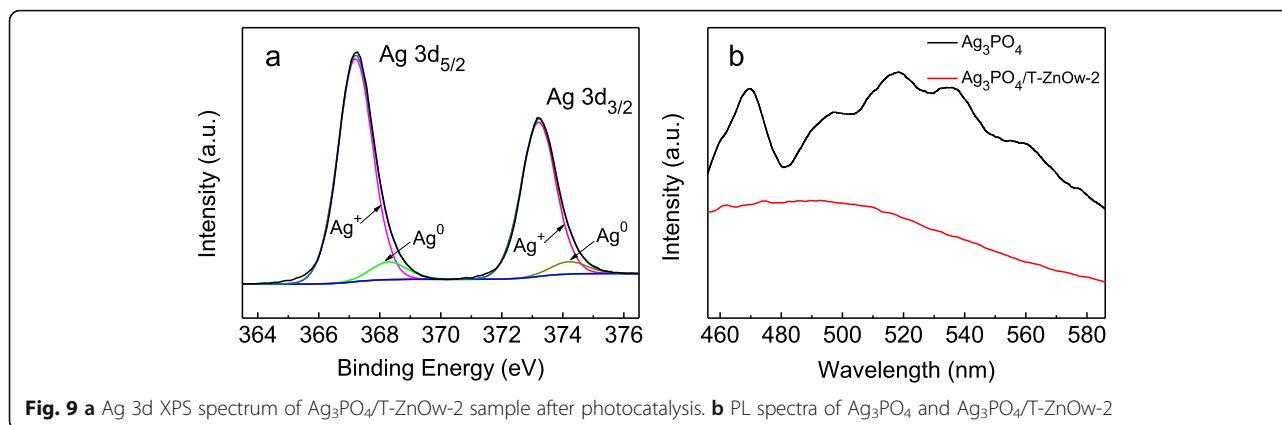
Fig. 7 Four successive cycling runs for degradation of RhB over Ag_3PO_4/T-ZnOw-2 and Ag_3PO_4

Scheme 1 Schematic diagram of the possible photocatalytic mechanism of Ag_3PO_4/T-ZnOw

Fig. 9 a Ag 3d XPS spectrum of Ag_3PO_4/T-ZnOw-2 sample after photocatalysis. **b** PL spectra of Ag_3PO_4 and Ag_3PO_4/T-ZnOw-2

The possible mechanism for the photocatalytic degradation of RhB could be proposed based on the above results, as shown in Scheme 1. The conduction band potential (CB – 0.32 eV) and valance band potential (VB 2.84 eV) of T-ZnOw were more negative than those of Ag_3PO_4 (CB 0.45 eV; VB 2.87 eV). The excited Ag_3PO_4 could produce electron-hole pairs under visible light illumination. Therefore, the photogenerated holes could shift from the VB of Ag_3PO_4 into the empty VB of T-ZnOw, which facilitated the effective separation of photogenerated electrons and holes. A part of photogenerated holes would react with the adsorbed H_2O to form ·OH as major active species, and the other part of holes adsorbed on the surface of the heterostructure could directly participate in the photodegradation of RhB. However, the CB potential of Ag_3PO_4 was 0.45 eV, which was higher than the reduction potential of $O_2/·O_2^-$ (– 0.33 eV) [29]. The photogenerated electrons on the conduction band of Ag_3PO_4 could not react with dissolved oxygen to form $·O_2^-$. A small amount of metallic Ag could be formed by the reaction between Ag^+ from Ag_3PO_4 and photogenerated electrons by visible light illumination, which could be proved by the XPS spectrum of Ag_3PO_4/T-ZnOw-2 after illumination for 50 min in photocatalytic reaction. Figure 9a showed the Ag3d XPS spectrum of Ag_3PO_4/T-ZnOw-2 after photocatalysis for 50 min. The peak at 367.2 and 373.2 eV could be attributed to Ag^+ ions, and the peak at 368.3 and 374.2 eV was assigned to the metallic Ag [11]. Then, photogenerated electrons on the conduction band of Ag_3PO_4 could transfer to metallic Ag, thus inhibiting the recombination of electron-hole pairs. Furthermore, the photogenerated electrons could be captured by dissolved oxygen to form $·O_2^-$, which played one of the major roles in the photodegradation of RhB. All of these photogenerated reactive species (·OH, $·O_2^-$, and h^+) could react with RhB to form CO_2 and H_2O and finally enhance the photocatalytic performance for degradation of RhB. Figure 9b presented the PL spectra of Ag_3PO_4 and Ag_3PO_4/

T-ZnOw-2 with the excitation wavelength of 355 nm. Compared with pure Ag_3PO_4, the intensity of Ag_3PO_4/T-ZnOw-2 revealed a decrease in fluorescence, which was mainly attributed to the efficient charge carrier transfer between Ag_3PO_4 and T-ZnOw. The PL results were consistent with the proposed photocatalytic mechanism.

Conclusions

In summary, Ag_3PO_4/T-ZnOw heterostructures were successfully fabricated by a facile in situ precipitation method. The Ag_3PO_4/T-ZnOw-2 catalyst exhibited superior photocatalytic activity for RhB degradation than pure T-ZnOw and possessed better stability and reusability compared with pure Ag_3PO_4. Under the optimum condition, Ag_3PO_4/T-ZnOw-2 showed the highest photocatalytic efficiency among the heterostructures and still possessed a degradation efficiency of 77.8% after four successive cycles. The efficient photocatalytic performance of Ag_3PO_4/T-ZnOw photocatalyst could be attributed to the enhanced visible light response. The Ag_3PO_4/T-ZnOw-2 photocatalyst also showed good stability. The investigation of the effect of different scavengers on degradation efficiency of RhB demonstrated that ·OH and $·O_2^-$ were the mainly active species. A possible mechanism of the photodegradation pathway for RhB was proposed. Ag_3PO_4/T-ZnOw may be one of the potential photocatalysts for the use in the treatment of water pollutants.

Tang *et al. Nanoscale Research Letters* (2020) 15:131

Page 9 of 10

Author details
[1]School of Chemical Engineering and Technology, North University of China, Taiyuan 030051, Shanxi, People's Republic of China. [2]Department of Chemistry and Chemical Engineering, Taiyuan Institute of Technology, Taiyuan 030008, Shanxi, People's Republic of China.

References
1. Hoffmann MR, Martin ST, Choi W, Bahnemann DW (1995) Environmental applications of semiconductor photocatalysis. Chem Rev 95:69–96
2. Chen X, Shen S, Guo L, Mao SS (2010) Semiconductor-based photocatalytic hydrogen generation. Chem Rev 110:6503–6570
3. Chen C, Ma W, Zhao J (2010) Semiconductor-mediated photodegradation of pollutants under visible-light irradiation. Chem Soc Rev 39:4206–4219
4. Li X, Wang D, Cheng G, Luo Q, An J, Wang Y (2008) Preparation of polyaniline-modified TiO_2 nanoparticles and their photocatalytic activity under visible light illumination. Appl Catal B Environ 81:267–273
5. Wang D, Duan Y, Luo Q, Li X, An J, Bao L, Shi L (2012) Novel preparation method for a new visible light photocatalyst: mesoporous TiO_2 supported Ag/AgBr. J Mater Chem 22:4847–4854
6. Wang Y, Jiang F, Chen J, Sun X, Xian T, Yang H (2020) In situ construction of CNT/CuS hybrids and their application in photodegradation for removing organic dyes. Nanomaterials 10:178
7. Güy N, Atacan K, Karaca E, Özacar M (2018) Role of Ag_3PO_4 and Fe_3O_4 on the photocatalytic performance of magnetic Ag_3PO_4/ZnO/Fe_3O_4 nanocomposite under visible light irradiation. Sol Energy 166:308–316
8. Lizama C, Freer J, Baeza J, Mansilla HD (2002) Optimized photodegradation of Reactive Blue 19 on TiO_2 and ZnO suspensions. Catal Today 76:235–246
9. Al-Sabahi J, Bora T, Al-Abri M, Dutta J (2016) Controlled defects of zinc oxide nanorods for efficient visible light photocatalytic degradation of phenol. Materials 9:238
10. Wang X, Wan X, Xu X, Chen X (2014) Facile fabrication of highly efficient AgI/ZnO heterojunction and its application of methylene blue and rhodamine B solutions degradation under natural sunlight. Appl Surf Sci 321:10–18
11. Pan J, Zhang X, Mei J, Wang S, You M, Zheng Y, Cui C, Li C (2017) The cotton cellulose nanofibers framework of Z-Scheme ZnO/Ag_3PO_4 heterojunction for visible-light photocatalysis. J Mater Sci: Mater El 28:17744–17749
12. Jang ES, Won JH, Hwang SJ, Choy JH (2006) Fine tuning of the face orientation of ZnO crystals to optimize their photocatalytic activity. Adv Mater 18:3309–3312
13. Wang Y, Wang Q, Zhan X, Wang F, Safdar M, He J (2013) Visible light driven type II heterostructures and their enhanced photocatalysis properties: a review. Nanoscale 5:8326–8339
14. Pirhashemi M, Habibi-Yangjeh A (2013) Simple and large scale one-pot method for preparation of AgBr-ZnO nanocomposites as highly efficient visible light photocatalyst. Appl Surf Sci 283:1080–1088
15. Liu J, Zou S, Lou B, Chen C, Xiao L, Fan J (2019) Interfacial electronic interaction induced engineering of ZnO-BiOI heterostructures for efficient visible-light photocatalysis. Inorg Chem 58:8525–8532
16. Shaker-Agjekandy S, Habibi-Yangjeh A (2016) Microwave-assisted one-pot method for preparation of ZnO/AgI nanocomposites with highly enhanced photocatalytic activity under visible-light irradiation. Desalin Water Treat 57:16015–16023
17. Kiantazh F, Habibi-Yangjeh A (2015) Ag_3VO_4/ZnO nanocomposites with an n-n heterojunction as novel visible-light-driven photocatalysts with highly enhanced activity. Mater Sci Semicond Process 39:671–679
18. Xiang Z, Zhong J, Huang S, Li J, Chen J, Wang T, Li M, Wang P (2016) Efficient charge separation of Ag_2CO_3/ZnO composites prepared by a facile precipitation approach and its dependence on loading content of Ag_2CO_3. Mater Sci Semicond Process 52:62–67
19. Ma S, Xue J, Zhou Y, Zhang Z (2014) Photochemical synthesis of ZnO/Ag_2O heterostructures with enhanced ultraviolet and visible photocatalytic activity. J Mater Chem A 2:7272–7280
20. Balachandran S, Prakash N, Thirumalai K, Muruganandham M, Sillanpää M, Swaminathan M (2014) Facile construction of heterostructured $BiVO_4$-ZnO and its dual application of greater solar photocatalytic activity and self-cleaning property. Ind Eng Chem Res 53:8346–8356
21. Tang C, Liu E, Fan J, Hu X, Kang L, Wan J (2014) Heterostructured Ag_3PO_4/TiO_2 nano-sheet film with high efficiency for photodegradation of methylene blue. Ceram Int 40:15447–15453
22. Bi Y, Ouyang S, Umezawa N, Cao J, Ye J (2011) Facet effect of single-crystalline Ag_3PO_4 sub-microcrystals on photocatalytic properties. J Am Chem Soc 133:6490–6492
23. Yi Z, Ye J, Kikugawa N, Kako T, Ouyang S, Stuart-Williams H, Yang H, Cao J, Luo W, Li Z, Liu Y, Withers RL (2010) An orthophosphate semiconductor with photooxidation properties under visible-light irradiation. Nat Mater 9:559–564
24. Katsumata H, Taniguchi M, Kaneco S, Suzuki T (2013) Photocatalytic degradation of bisphenol A by Ag_3PO_4 under visible light. Catal Commun 34:30–34
25. Bi Y, Ouyang S, Cao J, Ye J (2011) Facile synthesis of rhombic dodecahedral AgX/Ag_3PO_4 (X= Cl, Br, I) hetero-crystals with enhanced photocatalytic properties and stabilities. Phys Chem Chem Phys 13:10071–10075
26. Yan J, Wang C, Xu H, Xu Y, She X, Chen J, Song Y, Li H, Zhang Q (2013) AgI/Ag_3PO_4 heterojunction composites with enhanced photocatalytic activity under visible light irradiation. Appl Surf Sci 287:178–186
27. Li Y, Wang P, Huang C, Yao W, Wu Q, Xu Q (2017) Synthesis and photocatalytic activity of ultrafine Ag_3PO_4 nanoparticles on oxygen vacated TiO_2. Appl Catal B Environ 205:489–497
28. Liu W, Liu D, Wang K, Yang X, Hu S, Hu L (2019) Fabrication of Z-scheme Ag_3PO_4/TiO_2 heterostructures for enhancing visible photocatalytic activity. Nanoscale Res Lett 14:203
29. Wang P, Li Y, Liu Z, Chen J, Wu Y, Guo M, Na P (2017) In-situ deposition of Ag_3PO_4 on TiO_2 nanosheets dominated by (001) facets for enhanced photocatalytic activities and recyclability. Ceram Int 43:11588–11595
30. Jia Y, Ma Y, Zhu L, Dong J, Lin Y (2019) Efficient visible-light-responsive photocatalyst: hybrid TiO_2-Ag_3PO_4 nanorods. Chem Phys 521:1–4
31. Dong C, Wu K, Li M, Liu L, Wei X (2014) Synthesis of Ag_3PO_4-ZnO nanorod composites with high visible-light photocatalytic activity. Catal Commun 46:32–35
32. Wu M, Yan L, Li J, Wang L (2017) Synthesis and photocatalytic performance of Ag/AgCl/ZnO tetrapod composites. Res Chem Intermed 43:6407–6419
33. Liu H, Wu X, Li X, Wang J, Fan X (2014) Simple preparation of scale-like CuO nanoparticles coated on tetrapod-like ZnO whisker photocatalysts. Cninese J Catal 35:1997–2005
34. Zhong Y, Djurišić AB, Hsu YF, Wong KS, Brauer G, Ling CC, Chan WK (2008) Exceptionally long exciton photoluminescence lifetime in ZnO tetrapods. J Phys Chem C 112:16286–16295
35. Wan Q, Wang TH, Zhao JC (2005) Enhanced photocatalytic activity of ZnO nanotetrapods. Appl Phys Lett 87:083105
36. Dzhurinskii BF, Gati D, Sergushin NP, Nefedov VI (1975) Simple and coordination compounds. An X-ray photoelectron spectroscopic study of certain oxides. Russ J Inorg Chem 20:2307–2314
37. Liu B, Xue Y, Zhang J, Han B, Zhang J, Suo X, Mu L, Shi H (2017) Visible-light-driven TiO_2/Ag_3PO_4 heterostructures with enhanced antifungal activity against agricultural pathogenic fungi *Fusarium graminearum* and mechanism insight. Environ Sci: Nano 4:255–264
38. Shao N, Wang J, Wang D, Corvini P (2017) Preparation of three-dimensional Ag_3PO_4/TiO_2@MoS_2 for enhanced visible-light photocatalytic activity and anti-photocorrosion. Appl Catal B Environ 203:964–978
39. Wu M, Li Y, Deng Z, Su BL (2011) Three-dimensionally ordered macroporous titania with structural and photonic effects for enhanced photocatalytic efficiency. ChemSusChem 4:1481–1488

Tang *et al. Nanoscale Research Letters*   (2020) 15:131

Page 10 of 10

40. Wen X, Niu C, Ruan M, Zhang L, Zeng G (2017) AgI nanoparticles-decorated CeO_2 microsheets photocatalyst for the degradation of organic dye and tetracycline under visible-light irradiation. J Colloid Interface Sci 497:368–377

41. Rezaei M, Habibi-Yangjeh A (2013) Simple and large scale refluxing method for preparation of Ce-doped ZnO nanostructures as highly efficient photocatalyst. Appl Surf Sci 265:591–596

42. Wang H, Li S, Zhang L, Chen Z, Hu J, Zou R, Xu K, Song G, Zhao H, Yang J, Liu J (2013) Surface decoration of Bi_2WO_6 superstructures with Bi_2O_3 nanoparticles: an efficient method to improve visible-light-driven photocatalytic activity. CrystEngComm 15:9011–9019

43. Zhang L, Wong KH, Chen Z, Jimmy CY, Zhao J, Hu C, Chan C, Wong PK (2009) AgBr-Ag-Bi_2WO_6 nanojunction system: a novel and efficient photocatalyst with double visible-light active components. Appl Catal A Gen 363:221–229

44. Xian T, Di L, Sun X, Li H, Zhou Y, Yang H (2019) Photo-Fenton degradation of AO7 and photocatalytic reduction of Cr(VI) over CQD-decorated $BiFeO_3$ nanoparticles under visible and NIR Light irradiation. Nanoscale Res Lett 14:397

45. Zheng C, Yang H, Cui Z, Zhang H, Wang X (2017) A novel $Bi_4Ti_3O_{12}$/Ag_3PO_4 heterojunction photocatalyst with enhanced photocatalytic performance. Nanoscale Res Lett 12:608

46. Liu H, Li D, Yang X, Li H (2019) Fabrication and characterization of Ag_3PO_4/TiO_2 heterostructure with improved visible-light photocatalytic activity for the degradation of methyl orange and sterilization of *E.coli*. Mater Technol 34:192–203

47. Li C, Zhang P, Lv R, Lu J, Wang T, Wang S, Wang H, Gong J (2013) Selective deposition of Ag_3PO_4 on monoclinic $BiVO_4$(040) for highly efficient photocatalysis. Small 9:3951–3956

48. Chen Z, Wang W, Zhang Z, Fang X (2013) High-efficiency visible-light-driven Ag_3PO_4/AgI photocatalysts: Z-scheme photocatalytic mechanism for their enhanced photocatalytic activity. J Phys Chem C 117:19346–19352

49. Golzad-Nonakaran B, Habibi-Yangjeh A (2016) Photosensitization of ZnO with Ag_3VO_4 and AgI nanoparticles: novel ternary visible-light-driven photocatalysts with highly enhanced activity. Adv Powder Technol 27:1427–1437

Publisher's Note